J Mater Sci: Mater Electron (2017) 28:7769–7777
DOI 10.1007/s10854-017-6472-y

Green synthesis of silver nanoparticles embedded in polyaniline nanofibers via vitamin C for supercapacitor applications

Li Tang[1,2] · Fang Duan[1] · Mingqing Chen[1]

Received: 18 November 2016 / Accepted: 25 January 2017 / Published online: 13 March 2017

Abstract The silver nanoparticles with high dispersion on the surface of polyaniline (PANI/Ag) was acquired by reduction of silver nitrate with the assistance of vitamin C acting as an environmentally friendly reducing agent. The surface morphology of the PANI/Ag composite revealed the PANI nanofibers with bright spots of silver nanoparticles. Specifically, this study could open an avenue for environmentally friendly, simple and cost effective methods in the surface functionalization and generation of silver nanoparticles into the PANI chains. The PANI/Ag composite exhibited the excellent capacitive performance with a specific capacitance as high as 553 F g^{-1} at 1 A g^{-1} because of the synergic effect of PANI and silver nanoparticles, which was much higher than that of PANI (316 F g^{-1}). Moreover, its electrical conductivity was 215.8 S cm^{-1}. Eventually, the greatly enhanced capacitive performance was mainly attributed to the silver nanoparticles, which could increase the electrical conductivity and promote the electron transfer between the active components.

1 Introduction

Supercapacitors have attracted great interest for the important application in the area of electrochemical energy storage because of increasing demand of electric equipment and digital communication [1–8]. They store energy via two mechanisms: (a) electrochemical double layer capacitance (EDLC) of the carbon materials and (b) pseudocapacitance of metal oxides and conducting polymers. It is worth noting that conducting polymers can offer the advantages of lower cost compared with metal oxides, and high charge density compared to carbon materials [9, 10]. Hence, they have received a lot of research interest due to their high conductivity and have become trendy basic materials for advanced applications such as energy storage and batteries [11, 12]. Among various conducting polymers, polyaniline is recognized as one of the most promising pseudocapacitive materials, which is suitable for the next generation of supercapacitors due to the advantageous properties of high pseudocapacitance, high energy density, light weight, controllable electrical conductivity, low cost, environmental friendliness and facile synthesis [13, 14]. The excellent electrode materials for supercapacitor principally demand high surface area, electrochemical stability, and good electrical conductivity. The electrical conductivity of metals is much higher than that of PANI. Therefore, the extensive research work has been focused on enhancing the electrical conduction of PANI composite electrode materials by using metal doping.

Recently, the PANI/metal composites have been extensively investigated for supercapacitor applications. First, these hybrid materials are expected to display some synergistic properties between PANI and metal nanoparticles, making them potential candidates for application in several fields such as catalysis, sensors, memory devices, fuel cells and so on [15–17]. Second, the structure of PANI or metal nanoparticles can be well controlled by the experimental methods and the interaction of PANI and metal salts. Finally, the high surface-to-volume ratio of metal nanoparticles in these PANI/metal composites should result in

✉ Mingqing Chen
mq-chen@jiangnan.edu.cn

[1] The Key Laboratory of Food Colloids and Biotechnology Ministry of Education, School of Chemical and Material Engineering, Jiangnan University, Wuxi 214122, China

[2] Wuxi Tourism and Commerce Branch of Jiangsu Union Technical Institute, Wuxi 214035, China

a large number of binding sites [18]. The metal nanoparticles could exhibit excellent electronic properties because of their high surface area to volume ratio in the technological applications [19, 20]. Among metal nanoparticles, the silver nanoparticles could exhibit the highest electrical and thermal conductivities among all the metal nanoparticles. The hybrid nanocomposites integrated silver nanoparticles on the surface of PANI are particularly important due to their excellent electrochemical properties. Therefore, the PANI/Ag nanocomposites can display unique combinations of the complementary advantages of PANI and Ag nanoparticles, and have been widely used in the secondary batteries, fuel cells and supercapacitors [21–23]. Moreover, the implementation of green methods to synthesize Ag nanoparticles can be easily adapted to modern advancements in nanotechnology, relieve progressively the cost pressure, increase the efficiency of the synthesized material, and more importantly maximize the use of environmentally benign solvents and nontoxic chemicals [24, 25]. Thus, as an effort to minimize the impact of Ag on the environment and to act accordingly with the above mentioned goals of the green synthesis methods, Ag has been commonly used in its nanoparticles form while getting homogeneously dispersed/embedded inside polymeric matrices to form functionally advanced nanocomposites [26]. Therefore, the incorporating Ag nanoparticles by the green synthesis method into PANI chains can increase their electrical conductivity and electrochemical storage capacity.

Herein, the PANI/Ag composite was obtained by in situ reduction of nitric acid-doped PANI with the assistance of vitamin C as a nontoxic reducing agent, which the nanofibers with the nanoporous structure could offer a relatively larger surface area, thereby improving their capacitive performance and electrical conductivity for supercapacitors. PANI/metal nanofibres are suitable candidates for high-performance supercapacitors because of the high conductivity and low charge transfer resistance. In principle, it is the electrode material that directly determines specific capacitances, cycling stability and rates capability of supercapacitors. Compared with other PANI-based electrode materials (PANI/metal ions, PANI/metallic oxide and PANI/carbon materials), the PANI/metal electrode material for supercapacitors has the advantages in contrast with the other PANI-based electrode materials (PANI/metal ions, PANI/metallic oxide and PANI/carbon materials), because PANI as typical pseudocapacitive materials has high energy storage capacity and metal has high electrical and thermal conductivities. On the one hand, the electrochemical properties of the PANI/metal composite electrode were much superior than that of PANI/metal ions electrode materials [27–29]. On the other hand, the synthesis of PANI/metallic oxide electrode materials was more complicated, and PANI/metallic oxide electrode materials suffer from poor stability and poor electrical conductivity [30, 31]. Furthermore, although PANI/carbon materials (CNTs and graphene) showed the excellent electrochemical behavior, the fabrication cost of the carbon materials would limit their application potential [32–34]. In addition, the doping concentration of Ag is varied to determine its effect on the magnitude of its specific capacitance as the electrode material for supercapacitors.

2 Materials and methods

2.1 Materials

Aniline was distilled twice under vacuum and stored in the dark below 0 °C, and ammonium peroxydisulfate (APS), nitric acid, silver nitrate, Dimethylformamide (DMF) were of analytical grade. Vitamin C, acetylene black and polytetrafluoroethylene (PTFE) 60 wt% dispersion were obtained from Sigma–Aldrich. All chemicals were used as received without further purifications.

2.2 Preparation of materials

For the synthesis of PANI/Ag composite, aniline (0.913 ml) was sonicated for 15 min in 100 ml of 1 M HNO_3 solution. Afterward, X ml of 0.1 M $AgNO_3$ and 1 M HNO_3 mixture solution was added to the mixture. 2.282 g APS in 50mL of 1 M HNO_3 solution was added to the above mixture drop by drop while stirring the mixture at 0 °C for 12 h. Then X/2 ml of 0.1 M Vitamin C solution was added dropwise to the reaction mixture and stirred for 8 h. After that, the product was filtered and washed several times with double distilled water and ethanol. Lastly, it was vacuum-dried at 80 °C for 24 h. PANI was synthesized in 1 M HNO_3 by chemical oxidative polymerization techniques in an ice water bath. To study the effect of doping concentration of Ag on the specific capacitance of PANI/Ag, the resultant samples were denoted as PANI/Ag1, PANI/Ag2 and PANI/Ag3, where X is 20, 60 and 100 ml during the synthesis.

2.3 Electrochemical measurements

All the nanocomposites were electrochemically characterized by cyclic voltammetry (CV), galvanostatic charge–discharge (GCD) and an electrochemical impedance spectroscopy (EIS) study by using a CHI 730B electrochemical workstation system (Shanghai Chenhua Instrument Factory, China). The electrochemical behavior of an electrode material not only depends on the nature, conductivity and the porosity of the electrode materials but also on the nature of the electrolytes. The three-electrode system was employed for all measurements

using 3 M NaOH as the electrolyte, where the samples coated the nickel foam electrode, platinum foil and Ag/AgCl (satd. KCl) served as the working electrode, the counter electrode and the reference electrode, respectively. The mixture of 90 wt% active materials, 5 wt% acetylene black and 5 wt% PTFE (60 wt%) in N-Methylpyrrolidone was coated onto the nickel foam plate with a definite area of 1 cm^2 was used as the working electrodes. CV tests were measured at 10 mV s^{-1} scan rate within a voltage range of −0.4 to 0.6 V (vs. SCE) and the galvanostatic charge/discharge curves were recorded at the current density range of 1–5 A g^{-1}. EIS was conducted by applying an AC voltage with a 5 mV amplitude in a frequency range from 0.01 Hz to 100 kHz under open circuit potential conditions. The specific capacitance from the discharge plot can be calculated by using the following equation:

$$\text{Specific capacitance}\left(C_{sp}\right) = \frac{It}{\Delta v m}$$

where I/m represents the current density in A g^{-1}, Δv is the potential sweep in V, and t is the discharge time, in seconds.

The electrical conductivity of the samples were measured by conventional four-electrode probe methods with compressed pellets. The thickness of the pellets for conductivity measurements is from 1.0 to 1.5 mm. The electrical conductivity was calculating with the following equation:

$$\rho = \frac{\pi t}{\ln 2\,(V/t)}$$

$$\text{conductivity}\,(\sigma;\text{S/cm}) = \frac{1}{\rho}$$

where ρ is the resistivity (Ω cm), V is the measured voltage, I is the source current, and t is the thickness of the samples.

2.4 Characterization

The X-ray powder diffraction (XRD) was conducted by using the Rigaku Rotaflex D/Max diffractometer with Cu $K\alpha$ of wavelength $\lambda = 1.5418$ Å. The morphologies of the as-prepared samples were observed by scanning electron microscope (SEM) (Hitachi S-4800) and TEM (JEM-2100) at 200 KV. The Raman spectroscopy was carried out at an excitation wavelength of 532 nm from a He–Ne laser excitation source of a Renishaw Raman microscope. The UV–visible spectroscopy analysis was performed by dissolving all of the materials in DMF solvent by using a Perkin-Elmer, Lambda 750 spectrophotometer. The N_2 adsorption/desorption isotherms and pore size distribution curves were analyzed by the analyzer (ASAP2020 MP).

3 Results and discussion

3.1 SEM analysis

The FESEM images of the PANI, PANI/Ag1, PANI/Ag2 and PANI/Ag3 composites, are shown in Fig. 1, respectively. Figure 1a indicates that the pure PANI are characterized by the nanofibers with the diameters of about 50 nm, and the length of the fibers ranged from hundreds of nanometers to several micrometers. The formation of the nanofibers are due to the self-assembly of individual polymer or oligomers through π–π interaction, hydrogen bonding and Vander Walls forces between aniline oligomers which causes the formation of polymeric nanofibers [35]. However, some aggregations existed in the pure PANI. As seen in Fig. 1b, the PANI/Ag1 composite exhibited isolated aggregates of silver nanoparticles into the PANI matrix. Figure 1c shows the PANI/Ag2 composite consisted of Ag nanoparticles clusters, which equally dispersed throughout the PANI matrixes. In addition, many PANI nanofibers can join with others and form the branched structures or interconnected electric networks in the composite. But with increasing Ag loading, Fig. 1d exhibits the PANI/Ag3 composite had the obvious agglomeration of Ag nanoparticles. So the schematic illustration of the formation processes of the PANI/Ag composite is supposed and shown in Fig. 1e. The Ag has several positions for doping and tends to bind with nitrogen sites of PANI leading to interchain linkage between many adjacent PANI chains by coordination [36]. The high surface area to volume ratio of the Ag nanoparticles can provide the high charge/discharge rate and specific capacitance at the same time. Furthermore, it is worth noting that the PANI/Ag2 composite exhibits that Ag nanoparticles are uniformly covered with PANI chains with increasing Ag contents, and the nanofibers with the nanoporous structure can offer the relatively larger surface area. In brief, the nanofibers and porous structure are beneficial for supercapacitors, because they can reduce the diffusion resistance of the electrolyte into the electrode matrix [37].

3.2 TEM analysis

The surface morphologies of PANI and PANI/Ag2 composite are investigated by TEM, as shown in Fig. 2. Figure 2a shows the pure PANI nanofibers have been synthesized with hundreds of nanometers in length and 50 nm in width. And the Ag nanoparticles were distributed with a spherical shape on the surface of the PANI without agglomeration in Fig. 2b, which also was confirmed by X-ray diffraction. The average diameter of the Ag nanoparticles is in the range of 10–20 nm. It is possible to observe in the micrographs that the Ag nanoparticles are well dispersed in the polymeric matrix. The main reason for the highly dispersion of the

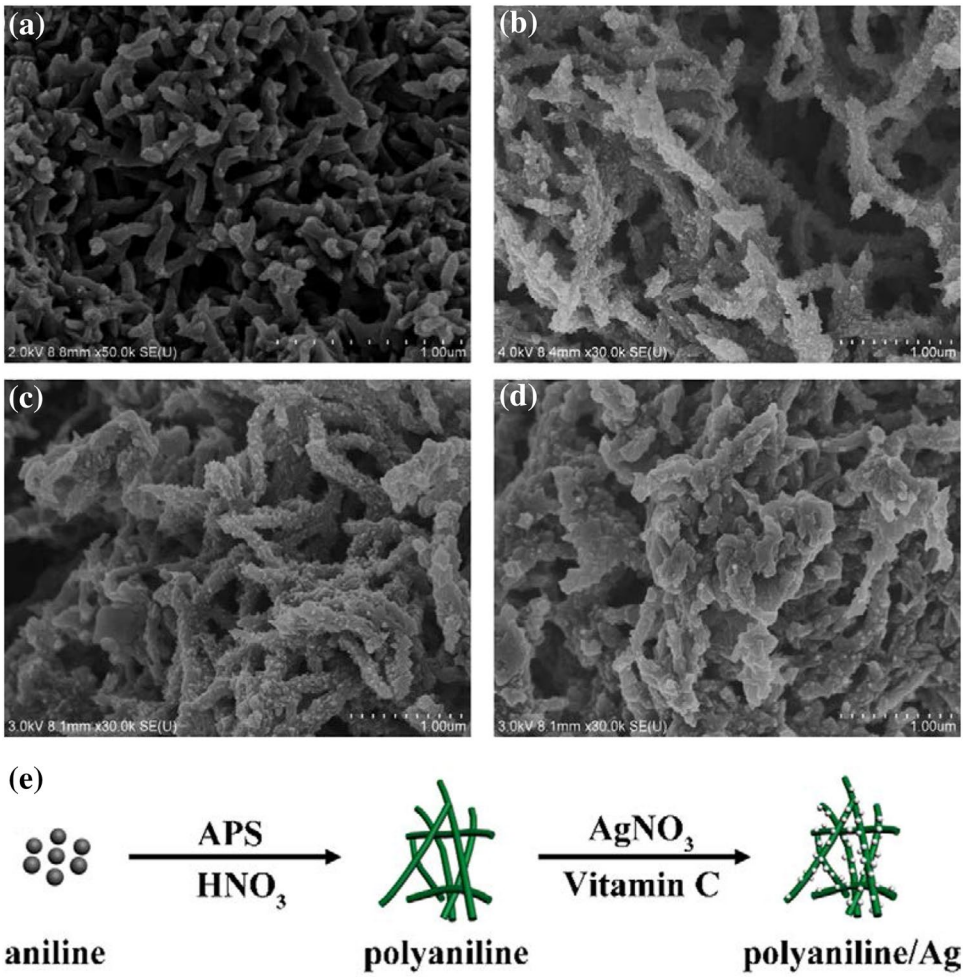

Fig. 1 FESEM images of **a** PANI, **b** PANI/Ag1, **c** PANI/Ag2 and **d** PANI/Ag3, and **e** the schematic illustration of the formation steps of PANI/Ag

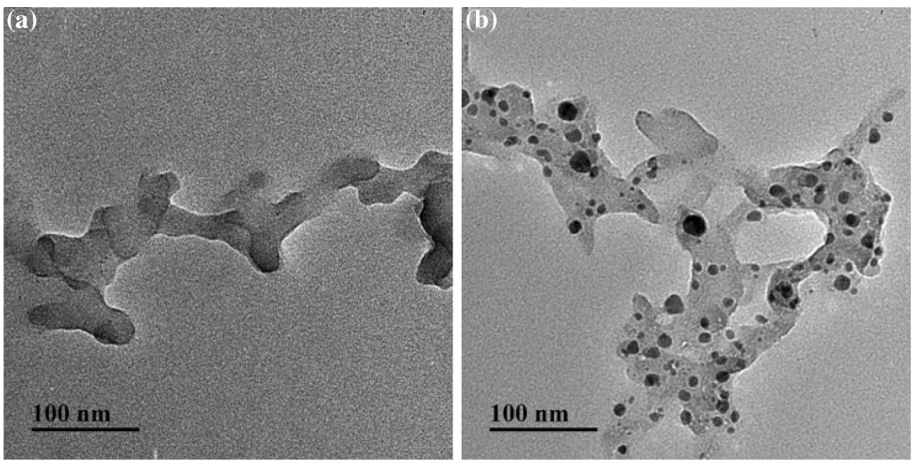

Fig. 2 TEM images of **a** PANI and **b** PANI/Ag2

Ag nanoparticles may due to the strong interaction between the polymer and the metal nanoparticles. Moreover, the Ag nanoparticles as a good electrical conductor tended to form clusters during the synthesis reactions due to their high surface energies, but they still kept their particle shapes on those clusters simply because of their electrochemical interactions with the PANI nanofibers. Furthermore, similarly formed Ag nanoparticles clusters were expected to exhibit distinctive size-dependent properties owing to their nanoparticles' narrow particle size distribution and facet

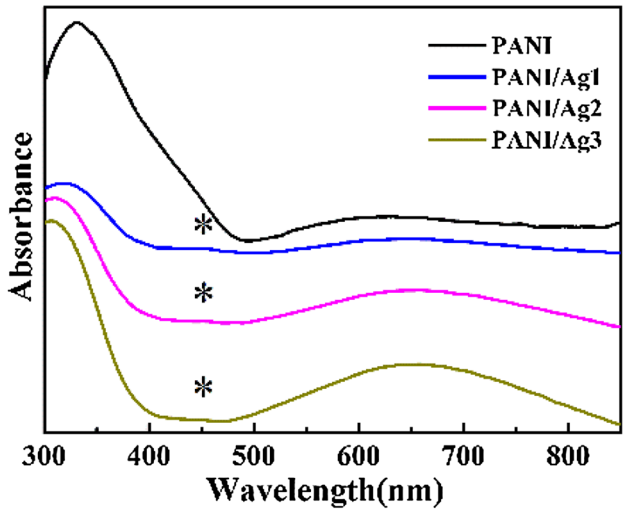

Fig. 3 UV–Vis spectra of **a** PANI, **b** PANI/Ag1, **c** PANI/Ag2 and **d** PANI/Ag3

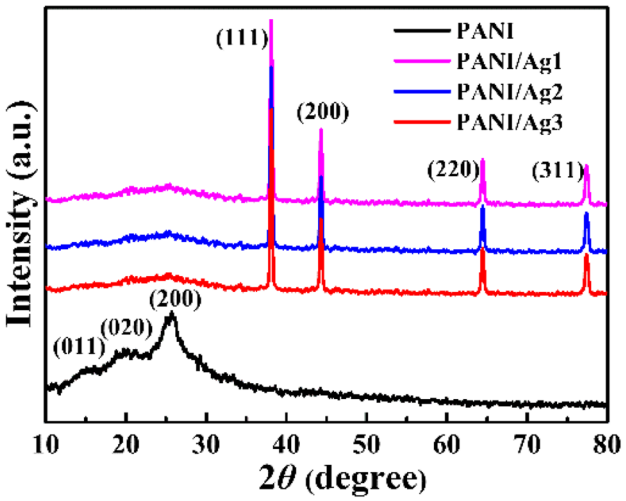

Fig. 4 XRD patterns of **a** PANI, **b** PANI/Ag1, **c** PANI/Ag2 and **d** PANI/Ag3

compositions [38], thus inducing a further improvement of capacitive performance.

3.3 UV–Visible Spectroscopy Analysis

Figure 3 shows the UV–Visible spectra of pure PANI, PANI/Ag1, PANI/Ag2 and PANI/Ag3 composites, respectively. PANI exhibited the two absorption bands at 330 and 630 nm. The band at 330 nm is attributed to the π–π^* transitions in the benzonoid units of PANI chains, while the other band at 630 nm is attributed to the exciton-like transition in quinonoid units. The spectrum of the PANI/Ag1 composite displayed three absorption peaks at 322, 450 and 638 nm, whereas the absorption spectra of the PANI/Ag2 and PANI/Ag3 composites exhibited three absorption peaks at 312, 450, 651 nm and 306, 450, 658 nm, respectively. And more importantly, the peak appeared at 450 nm for the PANI/Ag1, PANI/Ag2 and PANI/Ag3 composites, corresponding to the surface plasmon resonance of the silver nanoparticles that were embedded in the polymer matrix [39]. Compared with the pure PANI, the shifts of the two absorption bands may be due to the interaction of Ag nanoparticles and amine/imine units of PANI chains [40].

3.4 XRD analysis

The XRD patterns of the pure PANI, PANI/Ag1, PANI/Ag2 and PANI/Ag3 composites are shown in Fig. 4. The characteristic peaks of PANI appear at 15.1°, 20.6°, 25.3° corresponding to the (011), (020), and (200) crystalline plane, respectively [41]. For the PANI/Ag1 composite, the sharp crystalline peaks appearing at 38.10°, 44.25°, 64.38°, and 77.42° corresponded to the face-centered cubic (fcc) phase of silver (111), (200), (220), and (311), respectively [42]. The same crystalline peaks were observed for the PANI/Ag2 and PANI/Ag3 composites. The existence of sharp peaks in both PANI/Ag composites clearly indicates the presence of Ag nanoparticles in the composite with their crystalline nature, confirming the successfully incorporation of the silver nanoparticles into the PANI matrix. Moreover, it was observed that all of the XRD patterns show a broad peak at 2θ values of ~17–30°. This is mainly because of the amorphous behavior of PANI. Therefore, compared with the pure PANI the intensity of the characteristic peaks of PANI became weak because many Ag nanoparticles were uniformly distributed on the surface of the PANI nanofibers.

3.5 Raman spectroscopy

The Raman spectra of the pure PANI, PANI/Ag1, PANI/Ag2 and PANI/Ag3 composites are shown in Fig. 5. For the pure PANI, the characteristic peaks appear at 1171, 1488 and 1590 cm^{-1} are corresponding to the C–H bending, C=N stretching and C=C stretching respectively, which are the characteristic peaks of the quinoid segment. The other two peaks characteristic of PANI appearing at 1241 and 1618 cm^{-1} indicate the C–H bending and C–C stretching of the benzenoid ring [18]. Moreover, the characteristic band of C–$N^{\bullet+}$ at 1340 cm^{-1} demonstrates the formation of the radical cation on the doping and co-doping of PANI [43]. It is noteworthy that the C–N stretching (1220 cm^{-1}) and the quinoid C=C stretching (1590 cm^{-1}) are slightly shifted to lower values in the case of PANI/Ag1 (1216 and 1585 cm^{-1}), PANI/Ag2 (1212 and 1581 cm^{-1}) and PANI/

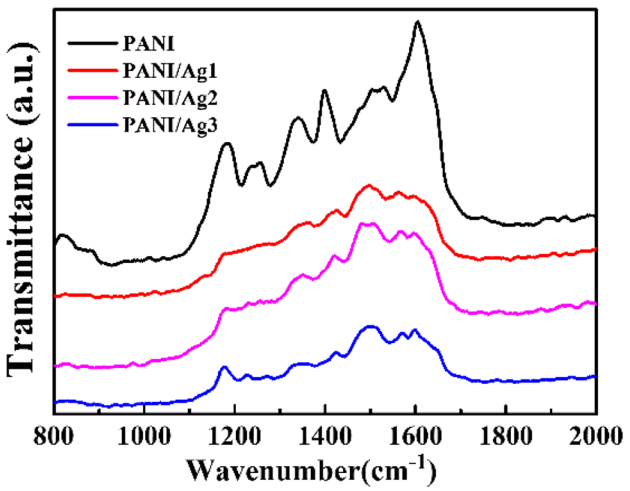

Fig. 5 Raman spectra of PANI, PANI/Ag1, PANI/Ag2 and PANI/Ag3

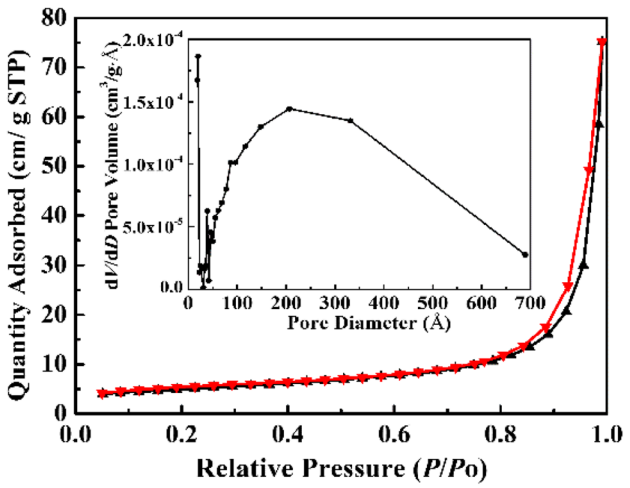

Fig. 6 N_2 adsorption/desorption isotherm plot and pore size distribution of PANI/Ag2

Ag3 (1209 and 1578 cm^{-1}), reconfirming that the interactions between PANI and silver nanoparticles readily occur. Furthermore, there is a slight shift in the peaks associated with C–N, C=N stretching indicating the interaction of PANI and Ag nanoparticles.

3.6 Surface area and pore size distribution

The N_2 adsorption/desorption isotherm plot and the pore size distribution of the PANI/Ag2 composite are shown in Fig. 6. The surface area calculated from the BET theory based on the isotherms for the PANI/Ag2 composite is 17.2 m^2/g, respectively. Moreover, the N_2 adsorption/desorption plot exhibits a H3-type hysteresis loop, confirming the existence of mesopores, which can be also confirmed by the pore size distribution curve in the inset. These mesoporous networks can provide low-resistance pathways through the porous structure, which is helpful to improve the charge transport and power capability [44]. These high specific surface and suitable pore size are the important factors for the large specific capacitance and high-rate charge/discharge ability. Hence, it is expected that the PANI/Ag2 composite has an excellent electrochemical performance.

3.7 Electrochemical analysis

The capacitive performances of the PANI, PANI/Ag1, PANI/Ag2 and PANI/Ag3 composites were measured by cyclic voltammetry, as shown in Fig. 7a. It was observed that the redox reaction takes place at the electrode–electrolyte interface which leads to the pseudocapacitance behavior. Compared with the pure PANI, the PANI/Ag1 composite shows additional anodic peak at 0.21 V because of the oxidation of Ag, which again proves the presence of Ag nanoparticles [39]. As the doping concentration of the Ag increases, the shift in the oxidation and reduction peaks of the PANI/Ag2 and PANI/Ag3 composites is also observed. It is noteworthy that the PANI/Ag2 composite exhibits a larger enclosed area, reflecting the larger specific capacitance. The enhanced specific capacitance in the PANI/Ag2 composite is attributed to the charge hopping through Ag nanoparticles that mediate the effective charge migration through the PANI chains [18]. It is well known that PANI with conjugated π-electron backbones can be oxidized or reduced more easily and more reversibly. As a result, the insertion of Ag nanoparticles into PANI can take place over the bulk volume of the polymer rather than just at the surface of PANI, and then a very large amount of charge carriers are generated per unit volume. Hence, the reason is that it can prevent the agglomeration of Ag nanoparticles and obtain the uniform dispersion over the entire PANI nanofibers.

Figure 7b gives the typical GCD curves of the pure PANI, PANI/Ag1, PANI/Ag2 and PANI/Ag3 composites. The specific capacitances of the pure PANI, PANI/Ag1, PANI/Ag2 and PANI/Ag3 composites obtained from the charge–discharge plots were 316, 476, 553, and 512 F g^{-1} at 1 A g^{-1}, respectively. The PANI/Ag2 composite showed the higher specific capacitance of 492 F g^{-1} at 2 A g^{-1}, 457 F g^{-1} at 3 A g^{-1}, 416 F g^{-1} at 4 A g^{-1} and 395 F g^{-1} at 5 A g^{-1}, as shown in Fig. 6c. As the Ag doping concentration increases, the specific capacitance increases from 476 F g^{-1} to 553 F g^{-1} for PANI/Ag1 composite to PANI/Ag2 composite, respectively. The better specific capacitance of PANI/Ag2 composite may be due to the following possible reasons: (a) the stronger interaction between PANI and Ag nanoparticles; (b) the uniform coating of Ag nanoparticles on the surface of PANI gives a superior

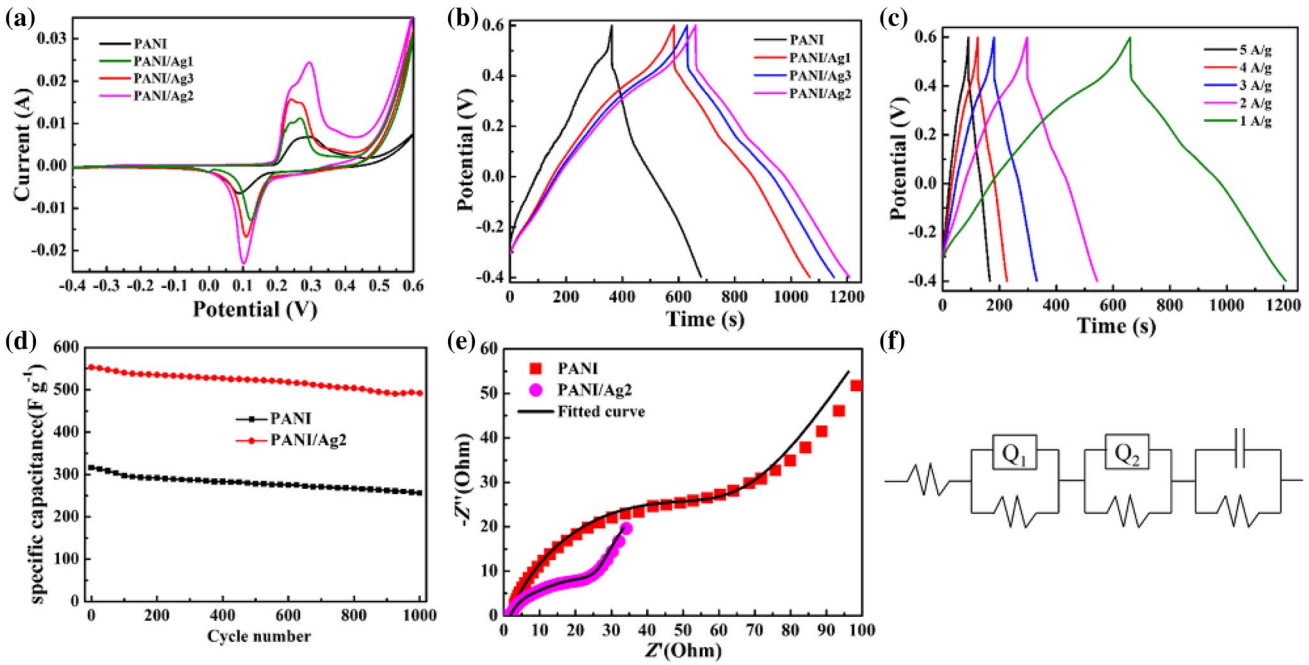

Fig. 7 Electrochemical performance of the electrodes: **a** CV curves of PANI, PANI/Ag1, PANI/Ag2 and PANI/Ag3 at 10 mV s^{-1}, **b** GCD curves of PANI, PANI/Ag1, PANI/Ag2 and PANI/Ag3 at 1 A g^{-1}, **c** GCD curves of PANI/Ag2 at different current density, **d** cycling life of PANI and PANI/Ag2, **e** EIS of PANI and PANI/Ag2 with the fitted curve and **f** the equivalent electrical circuit

structure for easy electrolyte accessibility. However, with further increment in the Ag doping, there is the decrease in the specific capacitance observed for the PANI/Ag3 composite, which may be due to the poorer contact between the electrolyte and PANI. This is because more Ag nanoparticles are covered with the surface of PANI which lowers the redox reaction rate of the active material [18]. The electrochemical redox reaction in the electrodes occurs at three-phase boundaries where the active material, the electrolyte and the nickel foam. Due to the inherent low electronic conductivity of PANI, the resistance to electron conduction from the nickel foam to the active materials is very high. But the presence of Ag nanoparticles on the PANI nanofibers can provide a least resistance path to electrons. Hence, the fast electron transport between the nickel foam and the active material can enhance the specific capacitance. However, when Ag content increases, it leads to the decrease in active site area and the utilization of PANI and hence the decrement in the specific capacitance.

It was observed that the PANI/Ag2 composite shows the higher specific capacitance than the other composites. The plot of specific capacitance vs. cycle number for PANI and PANI/Ag2 composite is shown in Fig. 6d. In order to evaluate the durability of cycle life, the charge–discharge test was continued to 1000 cycles at 1 A g^{-1} current density for each of the PANI and PANI/Ag2 composite respectively, showing specific capacitance retention of 81 and 90% of initial specific capacitance at the end. All the two materials exhibited a quick decrease of specific capacitance at the initial cycles, which may be due to the degradation of some undoped PANI or incompletely formed polymer. With increasing cycle number, the variation showed almost parallel behaviour to the cycle number axis. The decrease of the conductivity resulting form swelling and shrinkage of PANI may the principle reason for the lower specific capacitance. The higher cyclic stability of the PANI/Ag2 composite can be attributed to the extraordinary electrical conductivity of the composite electrode due to the formation of the conductive network by the effective doping effect in the PANI chains with Ag nanoparticles, which is due to the chemical linkage between PANI and Ag nanoparticles [20]. The integration of Ag nanoparticles leads to the formation of the network structure of the PANI chains and accordingly results in a slow volume expansion during charge–discharge. Hence, the long life-cycle stability of the PANI/Ag2 composite is a crucial parameter for their practical supercapacitor applications.

The EIS spectroscopy was performed to evaluate the electrode performance of the prepared materials in a particular electrolyte and the kinetics involved. It gives the information about the charge transport behavior of the electrode material at the electrode/electrolyte interface. The EIS plot has been represented in terms of a Nyquist plot, after fitting with an equivalent electrical circuit and is represented in Fig. 7e with the circuit shown in Fig. 7 f. The semicircle in the Nyquist plot is characteristic of a single

time constant circuit. The diameter of the semicircle gradually decreases from pure PANI to PANI/Ag2 composite, indicating a gradual increase of the available surface area with additional active sites for faradaic reactions, and fewer obstructions in the electron transfer process. These imperfect capacitors are signified by constant phase element (CPE). CPE replaces the ideal capacitor and defines inhomogeneities of the electrode surface in electrochemical capacitors. The CPE arises due to the rough electrode surface, different dimension of coating, inhomogeneous distribution of reaction sites with different activation energies, non-uniform current distribution due to edge effect etc. CPE follow the equation: [42] $Z=1/(j.\omega.C)^n$, where j is $(-1)^{1/2}$, ω is the angular frequency, C is the ideal capacitance and n is an empirical constant ($0 \le n \le 1$). When $n=1$, CPE acts as an ideal capacitor. Moreover, n is an important parameter to decide the superiority of an electrode material. Generally for the supercapacitor, $0.5 < n < 1$, and the closer the value of n is to one, the more superior is the electrode material. For PANI to PANI/Ag2, the value of n was determined to be 0.75 and 0.83, respectively, also assuring the excellent supercapacitive behaviour of PANI/Ag2 composite compared with PANI.

3.8 Electrical conductivity measurements

The electrical properties of the pure PANI, PANI/Ag1, PANI/Ag2 and PANI/Ag3 composites were studied by four-probe measurements at room temperature. The electrical conductivity of the composites mainly depends on both the oxidation state of PANI and the silver content. The pure PANI shows electrical conductivity of 1.3 S cm^{-1}, and the PANI/Ag1 and PANI/Ag2 composites show the electrical conductivity of 26.5 and 215.8 S cm^{-1}, respectively. With the formation of the Ag nanoparticles, the nitrogen atoms electron become deficient state, thus enhancing the electrical conductivity [45]. Hence, with the increase in the doping concentration of Ag, the increase in the electrical conductivity of the PANI/Ag composite may help to enhance the specific capacitance. But when Ag content increases, the electrical conductivity of PANI/Ag3 composite is 175.6 S cm^{-1}. It's all because that there is the decrease in active site area of the composite due to the agglomeration of Ag nanoparticles on the surface of PANI nanofibers. Hence, it leads to the decrement in the electrical conductivity [46, 47].

4 Conclusion

In summary, the polymeric supercapacitor material PANI/Ag composite has successfully been prepared by a simple and inexpensive technique, thus requiring less time for reducing silver nitrate and increasing the silver content in the PANI complexes. It achieved the highest specific capacitance of 553 F g^{-1} at 1 A g^{-1}, and demonstrated the good rate capability and excellent long-term cyclic stability because of the uniform coating of Ag nanoparticles on the surface of PANI nanofibers. Compared with the pure PANI, the PANI/Ag composite showed the enhanced electrical conductivity. The typical superior properties revealed that the PANI/Ag composite could be used as the promising electrode material for the fabrication of better supercapacitors.

Acknowledgements This study was supported by the National Natural Science Foundation of China (No.51302108 and 21571084).

References

1. R. Wang, Y. Ma, H. Wang, J. Key, D. Brett, S. Ji, S. Yin, P.K. Shen, J. Mater. Chem. A **4**, 5390–5394 (2016)
2. S.A. Ansari, N. Parveen, T.H. Han, M.O. Ansari, M.H. Cho, Phys. Chem. Chem. Phys. **18**, 9053–9060 (2016)
3. S. Konwer, J. Mater. Sci. **27**, 4139–4146 (2016)
4. H. Heydari, M.B. Gholivand, J. Mater. Sci. (2016) doi:10.1007/s10854-016-5962-7
5. X. Zhang, H. Chen, D. Fang, J. Solid State Electr **20**, 2835–2845 (2016)
6. Y. Bao, X. Zhang, X. Zhang, L. Yang, X. Zhang, H. Chen, M. Yang, D. Fang, J. Power Sources **321**, 120–125 (2016)
7. X. Zhang, L. Yang, F. Hao, H. Chen, M. Yang, D. Fang, Nanomaterials 5, 1985–1994 (2015)
8. X. Zhang, F. Hao, H. Chen, D. Fang, Mech. Mater **91**, 351–362 (2015)
9. H. Behniafar, K. Malekshahinezhad, A. Alinia-Pouri, J. Mater. Sci. **26**, 1–7 (2016)
10. H.K. Seo, S.A. Ansari, N. Parveen, S. Qadir, H. Fouad, H.S. Shin, M.H. Cho, S.G. Ansari, Z.A. Ansari, J. Mater. Sci. (2016) doi:10.1007/s10854-016-5910-6
11. H. Mahdavi, P.K. Kahriz, H.G. Ranjbar, T. Shahalizade, J. Mater. Sci. **27**, 7407–7414 (2016)
12. P.M. Kharade, S.M. Mane, S.B. Kulkarni, P.B. Joshi, D.J. Salunkhe, J. Mater. Sci. **27**, 1–7 (2016)
13. J.W. Lee, J.U. Lee, J.W. Jo, S. Bae, K.T. Kim, W.H. Jo, Carbon **105**, 191–198 (2016)
14. P. Bober, J. Stejskal, M. Trchová, J. Prokeš, Electrochim. Acta **122**, 259–266 (2014)
15. S. Kazemi, M. Kiani, R. Mohamadi, L. Eskandarian, Bull. Mater. Sci. 37, 1001–1006 (2014)
16. Y. Wankhede, S. Kondawar, S. Thakare, P.S. More, Adv. Mater. Lett. **4**, 89–93 (2013)
17. E. Detsri, J. Popanyasak, Colloids Surf. A **467**, 57–65 (2015)
18. D.S. Patil, J. Shaikh, S. Pawar, R. Devan, Y. Ma, A. Moholkar, J. Kim, R. Kalubarme, C. Park, P. Patil, Phys. Chem. Chem. Phys. **14**, 11886–11895 (2012)
19. F. Roussel, R.C.Y. King, M. Kuriakose, M. Depriester, A. Hadj-Sahraoui, C. Gors, A. Addad, J.-F. Brun, Synthetic Met. 199, 196–204 (2015)
20. M. Hosseini, M.M. Momeni, J. Mater. Sci. **45**, 3304–3310 (2010)
21. Y. Xie, Z. Song, S. Yao, H. Wang, W. Zhang, Y. Yao, B. Ye, C. Song, J. Chen, Y. Wang, Mater. Lett. **86**, 77–79 (2012)

22. P. Bober, M. Trchová, J. Prokeš, M. Varga, J. Stejskal, Electrochim. Acta **56**, 3580–3585 (2011)
23. L. Tang, F. Duan, M. Chen, RSC Adv. 6, 65012–65019 (2016)
24. D.K. Chandrasekharan, P.K. Khanna, T.V. Kagiya, C.K.K. Nair, Cancer Biother. Radio. 26, 249–257 (2011)
25. P. Gnanaprakasam, T. Selvaraju, RSC Adv. 5, 6892–6892 (2014)
26. M.F. Alam, A.A. Laskar, M. Zubair, U. Baig, H. Younus, J. Mol. Catal. B. 119, 78–84 (2015)
27. J. Li, M. Cui, Y. Lai, Z. Zhang, H. Lu, J. Fang, Y. Liu, Synthetic Met. 160, 1228–1233 (2010)
28. S. Dhibar, S. Sahoo, C.K. Das, R. Singh, J. Mater. Sci. **24**, 576–585 (2013)
29. H. Xu, J. Wu, C. Li, J. Zhang, X. Wang, Ionics **21**, 1163–1170 (2015)
30. P.M. Kharade, S.G. Chavan, D.J. Salunkhe, P.B. Joshi, S.M. Mane, S.B. Kulkarni, Mater. Res. Bull. **52**, 37–41 (2014)
31. Z. Pei, L. Ding, M. Lu, Z. Fan, S. Weng, J. Hu, P. Liu, J. Phys. Chem. C **118**, 9570–9577 (2014)
32. M.A. Bavio, G.G. Acosta, T. Kessler, J. Power Sources **245**, 475–481 (2014)
33. G. Otrokhov, D. Pankratov, G. Shumakovich, M. Khlupova, Y. Zeifman, I. Vasil'eva, A. Yaropolov, Electrochim. Acta **123**, 151–157 (2014)
34. N.A. Kumar, J.B. Baek, Chem. Commun. **50**, 6298–6308 (2014)
35. X.-S. Du, C.-F. Zhou, G.-T. Wang, Y.-W. Mai, Chem. Mater. **20**, 3806–3808 (2008)
36. F. Lorestani, Z. Shahnavaz, P.M. Nia, Y. Alias, N.S. Manan, Appl. Surf. Sci. **347**, 816–823 (2015)
37. G.M. Neelgund, E. Hrehorova, M. Joyce, V. Bliznyuk, Polym. Int. 57, 1083–1089 (2008)
38. S. Poyraz, I. Cerkez, T.S. Huang, Z. Liu, L. Kang, J. Luo, X. Zhang, ACS Appl. Mater. Inter. 6, 20025–20034 (2014)
39. S. Dhibar, C.K. Das, Ind. Eng. Chem. Res **53**, 3495–3508 (2014)
40. H. Chaudhari, D. Kelkar, Polym. Int. 42, 380–384 (1997)
41. V. Sunny, T. Narayanan, U. Sajeev, P. Joy, D.S. Kumar, Y. Yoshida, M. Anantharaman, Nanotechnology **17**, 4765–4772 (2006)
42. D. Ghosh, S. Giri, A. Mandal, C.K. Das, Appl. Surf. Sci. **276**, 120–128 (2013)
43. E. Gomes, Am M. Oliveira,, J. Polym. Sci. **2**, 5–13 (2012)
44. G. Nesher, M. Aylien, G. Sandaki, D. Avnir, G. Marom, Adv. Funct. Mater. **19**, 1293–1298 (2009)
45. M. Varga, J. Prokes, P. Bober, J. Stejskal, Electrical conductivity of polyaniline-silver nanocomposites, WDS, pp. 52–57
46. L. Xia, C. Zhao, X. Yan, Z. Wu, J. Appl. Polym. Sci. **130**, 394–398 (2013)
47. P. Xu, S.-H. Jeon, H.-T. Chen, H. Luo, G. Zou, Q. Jia, M. Anghel, C. Teuscher, D.J. Williams, B. Zhang, J. Phys. Chem. C **114**, 22147–22154 (2010)